Nano Energy 122 (2024) 109302

Contents lists available at ScienceDirect

Nano Energy

journal homepage: www.elsevier.com/locate/nanoen

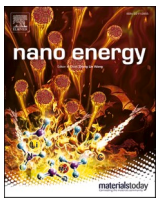

Simultaneous copper incorporation in core/shell-structured eco-friendly quantum dots for high-efficiency photoelectrochemical hydrogen evolution

Li Xia [a], Xin Tong [a,b,*], Yisen Yao [a,b], Zhihang Long [a], Mengke Cai [a], Lei Jin [a], Alberto Vomiero [c,d,**], Zhiming M. Wang [a,b,e,*]

[a] Institute of Fundamental and Frontier Sciences, University of Electronic Science and Technology of China, Chengdu 610054, PR China
[b] Yangtze Delta Region Institute (Huzhou), University of Electronic Science and Technology of China, Huzhou 313001, PR China
[c] Division of Materials Science, Department of Engineering Sciences and Mathematics, Luleå University of Technology, Luleå SE-97187, Sweden
[d] Department of Molecular Sciences and Nanosystems, Ca' Foscari University of Venice, Via Torino 155, Venezia Mestre 30170, Italy
[e] Institute for Advanced Study, Chengdu University, Chengdu 610106, PR China

ARTICLE INFO

Keywords:
Colloidal quantum dots
Environment-friendly
Core/shell system
Simultaneous copper incorporation
Solar hydrogen evolution

ABSTRACT

The rational design of elemental incorporation in colloidal eco-friendly core/shell quantum dots (QDs) holds the potential to synergistically tailor their electronic band structure and carrier kinetics for applications in forthcoming "green" and high-efficiency solar energy conversion. Herein, we have conducted simultaneous Cu incorporation in both the core and shell regions of environment-benign AgInSe (AISe)/ZnSe core/shell QDs to realize high-efficiency solar-driven photoelectrochemical (PEC) hydrogen evolution. It is verified that Cu incorporation in AISe core enables an upward shift in the position of the band edge relative to the ZnSe shell, which promoted the electron delocalization and extended the lifetime of exciton. Simultaneously, Cu incorporation in the ZnSe shell further results in the trapping of photoinduced holes from AISe core, leading to a decelerated recombination of carriers. The prepared Cu-AISe/ZnSe:Cu QDs with optimized optoelectronic properties have been successfully employed to fabricate QDs-PEC devices, delivering a maximum photocurrent density of 9.1 mA cm^{-2} under standard AM 1.5 G illumination (100 mW cm^{-2}). Our findings indicate that synchronous elemental incorporation in eco-friendly core/shell QDs is a promising strategy to achieve future high-performance solar-to-hydrogen conversion systems.

1. Introduction

With continuous consumption of fossil fuels, environmental pollution and climate change have become major issues in the development of human being [1]. Therefore, the pursuit of sustainable energy alternatives, including wind energy, tide energy, biomasses-derived energy, and solar energy, has gained paramount importance [2]. Among them, solar energy has garnered extensive attention due to its earth-abundant, eco-friendly and renewable features. A particularly promising avenue involves harnessing solar energy to produce hydrogen fuel, characterized by its high energy density and complete absence of carbon emissions [3]. As a solar-to-hydrogen generation system, photoelectrochemical (PEC) cells have attracted widespread attention over the last few decades, however, there are still many challenges impeding the practical implementation of PEC hydrogen production [4–6]. For instance, high-efficiency photoelectrodes are usually composed of high-cost semiconductors or precious metals, which are not conducive to the sustainable development of energy demand in the new era. In this context, it has become a research hotspot in recent years to exploit low-cost, earth-abundant, and high-performance photoelectric electrode materials [7–9].

Traditional semiconductor metal oxides with large band gap (such as ZnO and TiO_2) have been widely used as photoelectrode materials in PEC hydrogen production systems because of their low-cost, ecological friendliness and high stability [10–14]. However, owing to their wide band gap (3.0–3.2 eV), these semiconductor materials suffer from limited light absorption which only cover the ultraviolet (UV) region of the solar spectrum (~5%) [15]. Addressing this limitation, a crucial

* Corresponding authors at: Institute of Fundamental and Frontier Sciences, University of Electronic Science and Technology of China, Chengdu 610054, PR China
** Corresponding author at: Division of Materials Science, Department of Engineering Sciences and Mathematics, Luleå University of Technology, Luleå SE-97187, Sweden.
E-mail addresses: xin.tong@uestc.edu.cn (X. Tong), alberto.vomiero@ltu.se (A. Vomiero), zhmwang@uestc.edu.cn (Z.M. Wang).

https://doi.org/10.1016/j.nanoen.2024.109302
Received 13 November 2023; Received in revised form 9 January 2024; Accepted 13 January 2024
Available online 17 January 2024
2211-2855/© 2024 The Author(s). Published by Elsevier Ltd. This is an open access article under the CC BY license (http://creativecommons.org/licenses/by/4.0/).

strategy has arisen involving the incorporation of narrow band gap semiconductor materials to sensitize wide band gap metal oxides. This approach not only boosts solar spectrum utilization efficiency but also fosters heterostructure that facilitate charge separation and transport [16].

Colloidal quantum dots (CQDs) have been widely utilized in diverse solar technologies due to their unique size-dependent optical characteristics and broadband light absorption [17]. Example include QDs-sensitized solar cells (QDSCs), luminescent solar concentrators (LSC) and solar-driven PEC cells.[18] However, in recent years, most of the high-efficiency QDs-based PEC devices were fabricated using highly toxic and heavy metal (Cd, Pb etc.)-based QDs,[19–23] which may cause a series of environmental and human health issues [24–26]. Therefore, it is beneficial to explore environment-friendly QDs (e.g., I-III-VI Cu/Ag chalcogenides-based QDs) with excellent optoelectronic properties for realizing future "green" and high-efficiency PEC hydrogen production systems [27–33].

Among these environment-benign I-III-VI QDs, AgInSe (AISe) QDs are considered as promising candidates for solar technologies due to their narrow band gap (~1.24 eV in bulk), broad light absorbance (up to 900 nm) and considerable photoluminescence (PL) quantum yield (~40%) [34–36]. However, bare AISe QDs often show poor optoelectronic properties and chemical stability, as a result of the easily formed abundant surface defects/traps induced by the ambient environment (e.g., humidity and light) [37]. Constructing core/shell structured QDs, i.e. coating a shell material (usually ZnS and ZnSe) on the surface of the AISe core QDs, can significantly passivate these surface defects to enhance the optical properties and photo-/chemical-stability.[38,39] Nevertheless, the large lattice mismatch (about 11%) of AISe/ZnS QDs results in a large number of strain-induced defects between the interface of core and shell [40]. Encouragingly, AISe/ZnSe QDs with lower lattice mismatch have been developed and employed as effective building blocks in lighting devices and biological imaging applications [41–43]. However, owing to the typical type I electronic band structure of AISe/ZnSe QDs, the electrons and holes are well-confined in the core region, which is detrimental to the spatial separation of photo-excited electrons/holes because it lowers the charge extraction efficiency. Introducing transition metal elements (e.g., Cu, Mn) in core/shell QDs can effectively regulate the band structure and tune the photoinduced carrier dynamics toward high-efficiency solar energy conversion [44–46]. For example, Luo et al. demonstrated that the Cu incorporation in I-III-VI Zn-In-Se core QDs enabled obviously broadened optical absorption and prolonged exciton lifetime for effective charge carrier separation/transfer [47]. Moreover, incorporating transition metal in the shell region can also bring in impurity states to optimize the photoexcited charge dynamics in the core/shell QDs [48]. In particular, our group have previously verified that after incorporating Cu in the shell of a typical AgInS/ZnS core/shell QD system, the holes of core QDs were effectively trapped by the Cu^{+} states in the shell, thus resulting in suppressed charge recombination and boosted PEC H_2 evolution efficiency.[49].

In this work, Cu incorporation was simultaneously conducted in both the core and shell regions of "green" AISe/ZnSe core/shell QDs for application in PEC H_2 generation. Our findings demonstrate that Cu incorporation in the AISe core decreased the band offset between the core and the ZnSe shell, facilitating electron delocalization and mitigating charge recombination. Besides, the Cu incorporation in ZnSe shell promoted hole capture from the AISe core, leading to improved carrier extraction efficiency. Accordingly, the PEC devices fabricated using the optimized Cu-AISe/ZnSe:Cu QDs showed a saturated photocurrent density as high as 9.1 mA cm^{-2} and considerable operational stability under AM 1.5 G illumination (100 mW cm^{-2}).

2. Results and discussion

To prepare the Cu-AISe/ZnSe:Cu QDs, Cu incorporated AISe core QDs were first synthesized, followed by the growth of the ZnSe shell materials on the core QDs with additional Cu incorporation, as schematically shown in Fig. 1**a**. In parallel, the pristine AISe/ZnSe and Cu-incorporated AISe/ZnSe QDs were prepared as typical reference samples. Transmission electron microscope (TEM) investigations were performed to analyze the morphology of as-synthesized QDs, wherein the AISe and Cu-AISe core QDs (Figs. S1a-**b**) both exhibit quasi-spherical shapes with similar average sizes of (5.4 ± 0.3) and (5.4 ± 0.4) nm and the relevant HRTEM images exhibit a lattice spacing of 0.35 nm that is indexed to the (111) plane of AISe (Figs. S1c-**d**). As shown in Fig. 1**b-d,** the AISe/ZnSe, Cu-AISe/ZnSe and Cu-AISe/ZnSe:Cu QDs all exhibit quasi-spherical shapes with similar average sizes of (7.1 ± 0.6), (7.1 ± 0.7) and (7.1 ± 0.6) nm, respectively, indicating that the incorporation of Cu in both core and shell regions did not significantly impact the particle size of AISe/ZnSe QDs, while the obviously increased QD size proved the growth of ZnSe shell on AISe and Cu-AISe QDs. Fig. S2a displays the high-resolution TEM (HRTEM) images of AISe/ZnSe QDs, showing a clear lattice spacing (3.2 Å) indexed to the (002) plane of wurtzite (WZ) phase ZnSe, which suggests the growth of a comparatively thick WZ ZnSe shell on AISe core QDs.[41] Besides, this lattice spacing (3.2 Å) is also consistent with those measured in HRTEM images of Cu-AISe/ZnSe (Fig. S2b) and Cu-AISe/ZnSe:Cu QDs (Fig. 1**e**), demonstrating the preservation of the WZ-type crystal structure of the QD shell after Cu-incorporation. X-ray diffraction (XRD) measurements were conducted to further verify the crystal structure of AISe/ZnSe, Cu-AISe/ZnSe and Cu-AISe/ZnSe:Cu QDs, as depicted in Fig. 1**f**. Due to the growth of relatively thick ZnSe shell on AISe QDs, we observed six typical diffraction peaks indexed to the (100), (002), (101), (110), (103) and (112) planes of WZ phase ZnSe (JCPDS #01–089-2940) for AISe/ZnSe QDs. Similarly, the XRD patterns of Cu-AISe/ZnSe and Cu-AISe/ZnSe:Cu QDs after Cu core or shell incorporation still aligned well with the WZ phase ZnSe, which are in accordance with the HRTEM results and the selected area electron diffraction (SAED) patterns (Figs. S2c-**e**), implying that such low-concentration Cu-incorporation in both core and shell region of AISe/ZnSe QDs can retain their pristine ZnSe crystal structure. X-ray photoelectron spectroscopy (XPS) was carried out to investigate the chemical compositions of Cu-AISe/ZnSe:Cu QDs. Fig. S3 shows the XPS survey spectrum of Cu-AISe/ZnSe:Cu QDs, wherein the XPS signals of Zn 2p and Se 3d are notably more prominent than those of Cu 2p, Ag 3d, and In 3d, indicating the growth of a thick ZnSe shell on the core QDs, which is consistent with the elemental atom percentages of 33.7%, 41.0%, 8.4%, 7.4% and 9.5% for Zn, Se, Ag, In, and Cu in QDs (Table S1). Fig. 1**g-k** reveal the high-resolution XPS (HRXPS) spectra of Ag 3d, In 3d, Se 3d, Zn 2p, and Cu 2p in QDs, with characteristic peaks displayed at 373.3/368.1 eV, 452.3/445.4 eV, 55.7/54.0 eV, 1045.6/1024.3 eV, and 955.6/932.7 eV, respectively. Inductively coupled plasma-optical emission spectrometry (ICP-OES) results of Cu-AISe/ZnSe:Cu QDs respectively show the molar percentages of Cu, Ag, In, Se and Zn as 8.2%, 9.9%, 12.1%, 39.3% and 30.5% (Table S1), in agreement with XPS results, further demonstrating the formation of a thick ZnSe shell on AISe core with Cu incorporation.

To investigate the optical properties of QDs, we measured the ultraviolet-visible (UV–vis) absorption spectra of the AISe/ZnSe, Cu-AISe/ZnSe and Cu-AISe/ZnSe:Cu QDs in solution (Fig. 2**a**). In comparison to the original AISe/ZnSe QDs, the absorption edge of Cu-AISe/ZnSe QDs shifted towards a longer wavelength, most likely because the introduction of Cu can lead to a decreased band gap of core QDs, as verified by the absorption spectra for AISe and Cu-AISe core QDs (Fig. S4a). When Cu was incorporated in the ZnSe shell, the absorption edge of Cu-AISe/ZnSe:Cu QDs further red-shifted due to the formation of ZnSe:Cu shell possessing relatively narrow band gap compared to the original ZnSe shell, which is more prominent in the QD samples with a higher Cu incorporation concentration, as exhibited in Fig. S5a [49]. Tauc plots derived from the QDs' absorption spectra can roughly determine the approximate optical band gap values of AISe/ZnSe, Cu-AISe/ZnSe, and Cu-AISe/ZnSe:Cu QDs as a qualitative support to the data, which were assessed to be 2.35 eV, 2.32 eV and 2.28 eV,

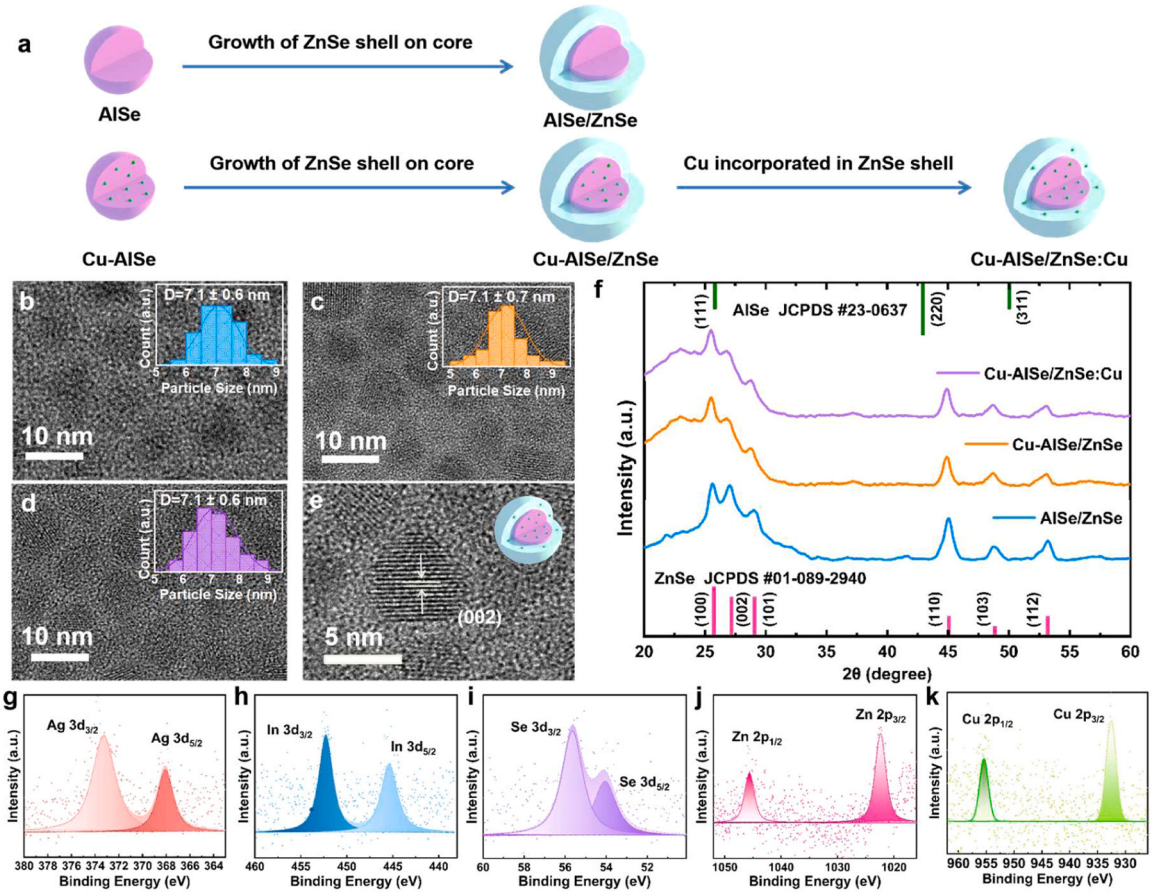

Fig. 1. (a) Schematic diagram for the preparation of Cu-AISe/ZnSe:Cu QDs. TEM images of (b) AISe/ZnSe, (c) Cu-AISe/ZnSe and (d) Cu-AISe/ZnSe:Cu QDs with inset size distribution histograms. (e) HRTEM image of Cu-AISe/ZnSe:Cu QDs. (f) XRD patterns of AISe/ZnSe, Cu-AISe/ZnSe and Cu-AISe/ZnSe:Cu QDs. HRXPS spectra of (g) Ag 3d, (h) In 3d, (i) Se 3d, (j) Zn 2p and (k) Cu 2p in Cu-AISe/ZnSe:Cu QDs.

respectively (Fig. 2**b**). It is also found that the band gap of QDs gradually reduced with a higher degree of Cu shell incorporation (Fig. S5b). Fig. 2**c** shows the PL spectra of QDs in solution, in which the AISe/ZnSe QDs exhibited an PL peak at ~700 nm, while the Cu-AISe/ZnSe QDs displayed a red-shifted PL peak at approximately 720 nm, which is in accordance with the results of the absorption spectra. After incorporation Cu in the ZnSe shell, the PL peak of the prepared Cu-AISe/ZnSe:Cu QDs red-shifted to ~730 nm, which is ascribed to the introduction of the Cu^+ state in ZnSe shell that affected the overall photo-induced charge dynamics in this type of core/shell QDs. Specifically, the emission peak can be further red-shifted with increasing Cu incorporation concentration (Fig. S6a) [50].

To investigate carrier kinetics of AISe/ZnSe core/shell QDs with synchronous Cu incorporation, transient PL decays of the QDs suspended in toluene were recorded, as illustrated in Fig. 2**d**. The average exciton lifetimes (τ_{av}) were derived through fitting a tri-exponential function (Table S2). As compared to the AISe/ZnSe QDs (τ_{av}=216 ns), the average exciton lifetime of Cu-AISe/ZnSe QDs was greatly extended to 466 ns, which may be attributed to the introduction of Cu that led to a longer lifetime of the incorporation-related emission and band position-correlated electron delocalization.[51] When Cu was incorporated into the shell of Cu-AISe/ZnSe QDs, the average exciton lifetime of QDs further increased to 706 ns, which is owing to Cu^+ state in the shell that trapped the holes from the core QDs for efficient electron-hole separation [52]. However, Figs. S6b-**d** show that the exciton lifetime of QDs decreased when the Cu introduction concentration increased to a certain amount, which is ascribed to the emerging hole scattering centers for further non-radiative recombination.[49] Therefore, Cu introduction in both the core and shell regions of AISe/ZnSe QDs can optimize the optical characteristics and promote the transfer/separation of photogenerated electrons and holes.

UV photoelectron spectroscopy (UPS, He I, 21.21 eV) was used to estimate the band positions of QDs and endorse the charge transfer in the Cu-AISe/ZnSe:Cu QDs-sensitized TiO_2 photoelectrodes (Figs. S7a-**c**). According to the high-resolution UPS (HRUPS) spectra, the cut-off of high and low binding energy for the QDs were measured to be 16.57 eV and 1.25 eV, respectively. It was thus calculated that the Fermi level and the valence band maximum were − 4.64 eV and − 5.89 eV versus vacuum (E_{vac}). Based on the valence band maximum position and the band gap obtained in Fig. 2**b**, the conduction band minimum was calculated as − 3.61 eV versus vacuum. Consequently, Fig. S7d schematically illustrates that the Cu-AISe/ZnSe:Cu QDs and TiO_2 can form a type II band alignment to facilitate the charge carrier separation and transfer [53].

To demonstrate the effect of Cu introduction on the delocalization of photoexcited electron in AISe/ZnSe QDs, we combined the UPS results and absorption spectra of AISe and Cu-AISe core QDs to study the band position variation between the core and shell. Tauc plots obtained from the absorption spectra roughly determined the optical band gaps of AISe and Cu-AISe QDs to be ~2.28 eV and 2.26 eV (Fig. S4b). Based on the high/low binding energy cut-off from UPS results of the core QDs (Fig. 2**e-h** and Fig. S8), the positions of the conduction band minimum and valence band maximum for AISe and Cu-AISe core QDs were calculated to be − 4.39/− 6.67 eV and − 4.20/− 6.46 eV, respectively, as illustrated in Fig. 3**a**.

In this case, the conduction band offset between Cu-incorporated AISe core QDs and ZnSe shell is smaller than that of the original AISe core QDs, which is more conducive to the delocalization of electrons into the shell region. Density functional theory (DFT) calculations were also

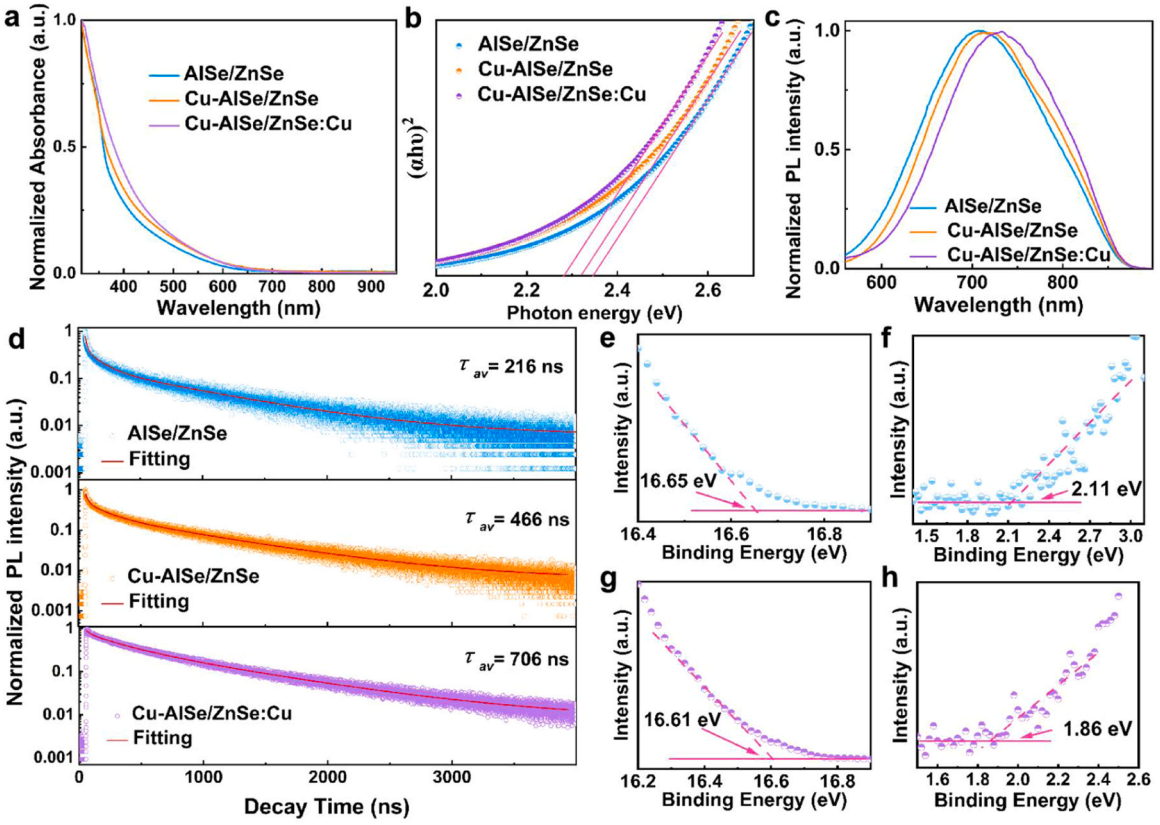

Fig. 2. (a) UV–vis absorption spectra and corresponding (b) Tauc plots of AISe/ZnSe, Cu-AISe/ZnSe and Cu-AISe/ZnSe:Cu QDs. (c) Steady-state PL spectra and (d) Time-resolved PL decay curves of AISe/ZnSe, Cu-AISe/ZnSe and Cu-AISe/ZnSe:Cu QDs. HRUPS spectra of AISe core QDs: (e) high and f) low binding energy cut-off. HRUPS spectra of Cu-AISe core QDs: (g) high and h) low binding energy cut-off.

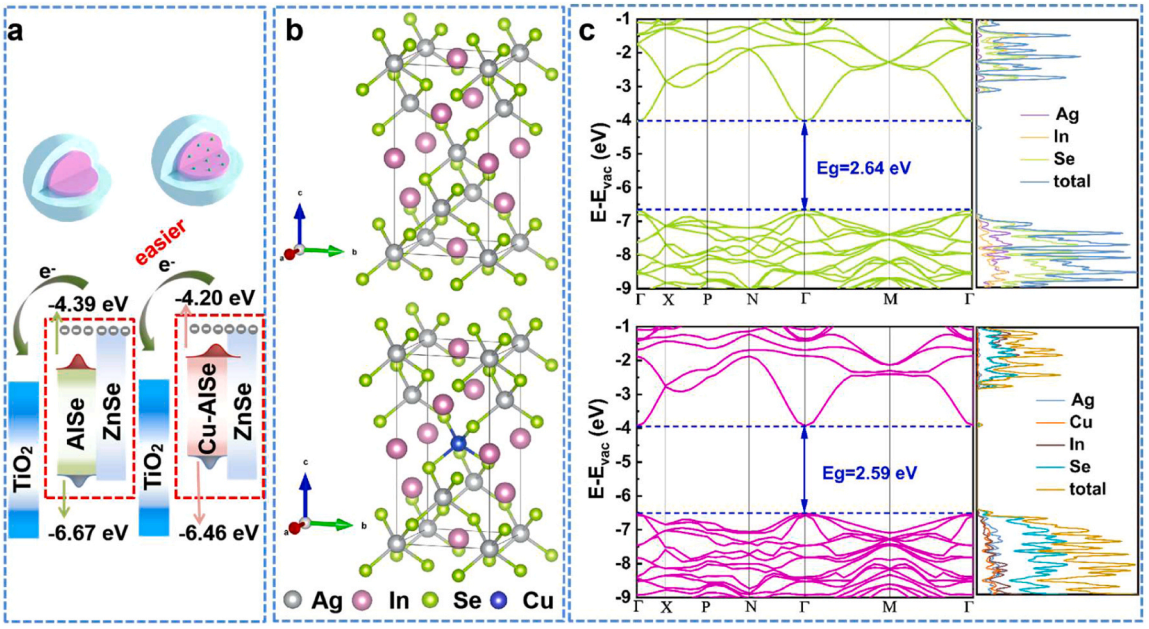

Fig. 3. (a) Schematic diagrams and band positions of AISe and Cu-AISe core QDs coated with ZnSe shell and the charge transfer from core/shell QDs to TiO_2. (b) Atomic structures of AISe and Cu-AISe QDs used in DFT calculations. (c) Electronic band structures and density of states (DOS) of AISe and Cu-AISe QDs calculated, where the energy level was aligned with respect to the vacuum level (E_{vac}).

used to study the electronic band structure of QDs and verify this conclusion. Fig. 3**b** displays the original electronic structure of AISe with a unit cell consisting of 4 Ag, 4 In and 8 Se atoms. As exhibited in Fig. 3**c**, the direct band gap energy of AISe was calculated to be 2.64 eV, while the band gap energy of Cu-AISe after Cu incorporation decreased to 2.59 eV, which is almost consistent with the experimental optical band

gap values. Moreover, after the introduction of Cu atomic orbitals via Cu incorporation, the band edge position of Cu-AISe was observed to slightly move upward, which has also been demonstrated by the UPS analysis. The theoretical results further confirm that the Cu incorporation can concurrently decrease the band gap and shift up the band edge position of AISe core, resulting in easier electrons delocalization into the ZnSe shell region.

As-synthesized QDs were used as light harvesters to sensitize TiO_2 for the fabrication of QDs-photoelectrodes via an electrophoretic deposition (EPD) technique. The cross-sectional scanning electron microscope (SEM) images of the assembled Cu-AISe/ZnSe:Cu QDs-sensitized TiO_2 photoanode were shown in Fig. 4**a**, in which the film thickness of QDs-TiO_2 was estimated to be ~17.1 μm. Fig. 4**a and S9** exhibit the EDS spectra and elemental mapping of QDs-TiO_2 photoanodes, where all components of the QDs were presented and uniformly distributed throughout the TiO_2 mesoporous film, confirming the successful sensitization of TiO_2 by Cu-AISe/ZnSe:Cu QDs. Fig. 4**b** schematically depicts the charge dynamics mechanism of Cu-AISe/ZnSe:Cu QDs/TiO_2 heterostructures, wherein the pristine AISe/ZnSe QD itself possesses a type-I band structure, while it can still form a type-II band alignment with TiO_2 for effective carrier separation/transfer. After Cu incorporation in AISe core, the band gap value and band edge position of Cu-AISe core QDs were changed, reducing the band offset with ZnSe shell to promote effective delocalization of electrons in the entire spatial core/shell structure and improve the photoinduced electron injection efficiency from QDs into TiO_2. With subsequent Cu incorporation in the ZnSe shell, the generated Cu^+ impurity states can trap the photogenerated holes from core and accelerate the hole transfer from QDs to the electrolyte, thus further suppressing the charge carrier's recombination in such QDs-TiO_2-based photoelectrodes.

To further explore the photoinduced charge kinetics associated with QDs-TiO_2 heterostructures, time-resolved PL spectra for three types of QDs/TiO_2, QDs/ZrO_2 and QDs/ZrO_2-elec (with electrolyte) electrodes were measured, in which the charge transfer between QDs and ZrO_2 is

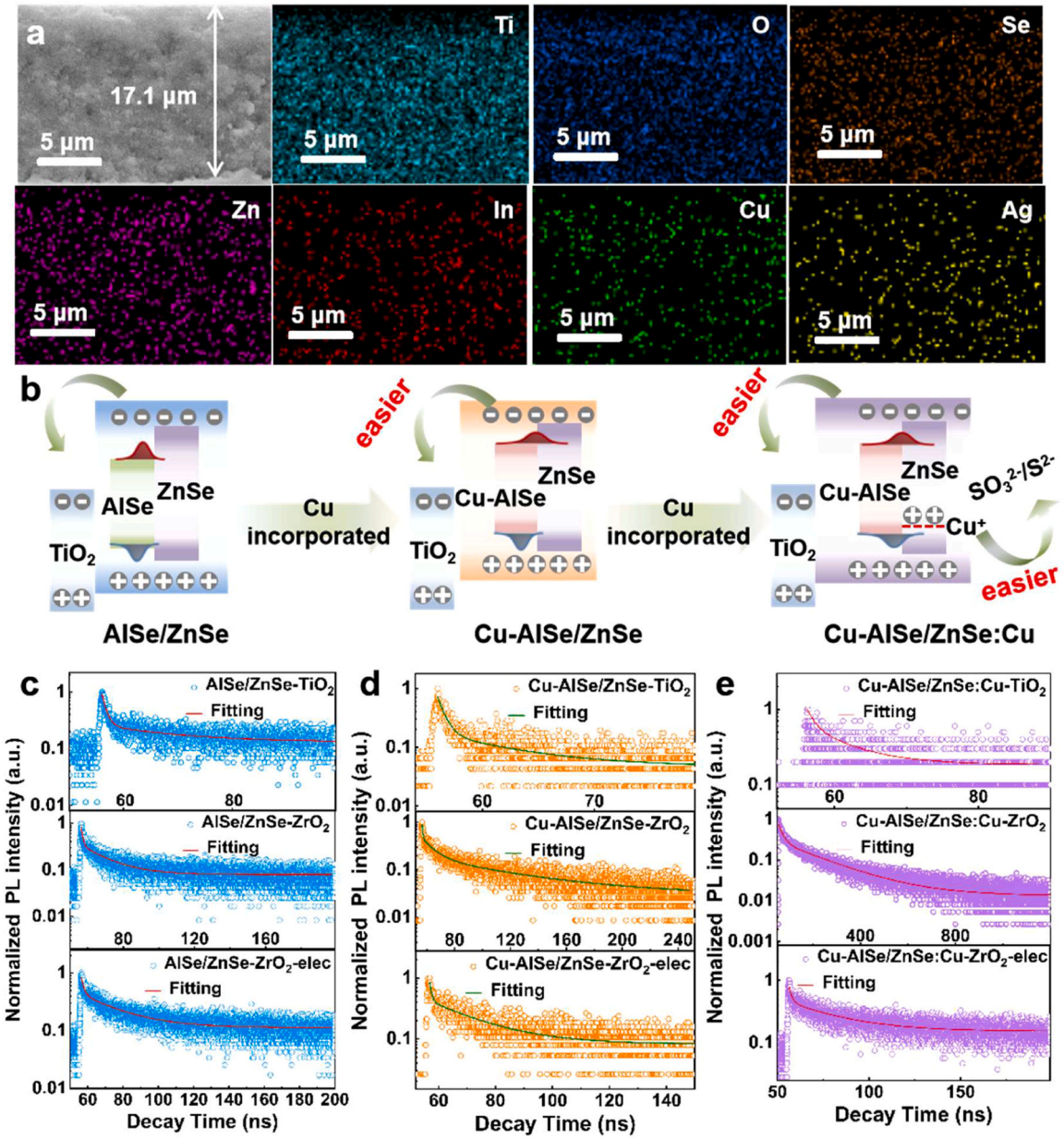

Fig. 4. (a) Cross-sectional SEM image and EDS elemental mapping (Ti, O, Se, Zn, In, Cu and Ag) of Cu-AISe/ZnSe:Cu core/shell QDs-TiO_2 heterostructures. (b) Schematic diagrams of the carrier kinetics mechanism in three types of QDs/TiO_2 heterostructures. Time-resolved PL spectra of (c) AISe/ZnSe, (d) Cu-AISe/ZnSe and (e) Cu-AISe/ZnSe:Cu QDs-modified TiO_2 and ZrO_2 (in the presence or absence of electrolyte).

forbidden because of the relatively large band gap of ZrO_2 (~6 eV) [54]. The transient PL decay curves and fitted exciton lifetime data of all QDs-TiO_2 or ZrO_2 were shown in Fig. 4**c-e** and recorded in Table S3, wherein the transient PL decay of all QDs/TiO_2 photoanodes was much faster than that of the QDs/ZrO_2 heterostructures due to effective charge transfer from QDs to TiO_2. According to the obtained exciton lifetime values of QDs/TiO_2 and QDs/ZrO_2, the electron transfer rate can be calculated by the following formula:[55].

$$K_{et} = \frac{1}{\tau_{QDs/TiO_2}} - \frac{1}{\tau_{QDs/ZrO_2}} \quad (1)$$

As summarized in Table S3, the electron transfer rate of Cu-AISe/ZnSe QDs-photoelectrodes (2.48 $\times 10^8$ s^{-1}) was much higher than that of the sample based on pristine AISe/ZnSe QDs (1.66 $\times 10^8$ s^{-1}), suggesting that the introduction of Cu into the core could cause the effective electron delocalization into the shell for enhanced carrier transfer from QDs to TiO_2. At the same time, after incorporation Cu in the shell, we observed that the electron transfer rate of Cu-AISe/ZnSe:Cu QDs-photoelectrodes (2.66 $\times 10^8$ s^{-1}) was slightly higher than that of the Cu-AISe/ZnSe QDs, indicating that the created Cu-related impurity states in the shell could further inhibit the charge recombination. Besides, the corresponding hole transfer rate can be estimated by testing the PL lifetime of all QDs-ZrO_2 samples with/without the presence of electrolyte and calculated using the following equation:

$$K_{ht} = \frac{1}{\tau_{QDs/ZrO_2(electrolyte)}} - \frac{1}{\tau_{QDs/ZrO_2}} \quad (2)$$

Consistently, Table S4 shows that the hole transfer rate of the Cu-AISe/ZnSe:Cu QDs-based photoanode (0.81 $\times 10^8$ s^{-1}) was higher than the Cu-AISe/ZnSe QDs-based photoelectrode (0.55 $\times 10^8$ s^{-1}) without Cu shell incorporation, thus testifying the improved hole transfer of QDs by Cu shell incorporation.

These fabricated QDs-sensitized TiO_2 photoelectrodes (working electrodes) were used in a typical PEC system to conduct hydrogen generation, and the operating principle of a QDs-PEC cell was illustrated in Fig. S10. The PEC performance of different QDs-based photoanodes with hole scavenger was evaluated by testing their linear scan voltammetry (LSV) curves, i.e., photocurrent density-applied bias (*J-V*) versus reversible hydrogen electrode (RHE), in the dark, under continuous and chopped illumination (1 sun, AM 1.5 G, 100 mW·cm^{-2}), as shown in Fig. 5**a-c**. Specifically, the AISe/ZnSe QDs-TiO_2 photoanode delivered a saturated photocurrent density of 4.5 mA·cm^{-2} (Fig. 5**a**), while after a certain amount of Cu atoms was incorporated in the core QDs, the Cu-AISe/ZnSe QDs-TiO_2 photoanode exhibited a significantly improved photocurrent density of 7.2 mA·cm^{-2} (Fig. 5**b**), which is attributed to the effect of Cu incorporation in the core for improved photogenerated electron transfer. After Cu incorporation into ZnSe shell, the saturated photocurrent density of Cu-AISe/ZnSe:Cu/TiO_2 photoelectrode further increased to 9.1 mA·cm^{-2} (Fig. 5**c**) due to that the Cu-related impurity

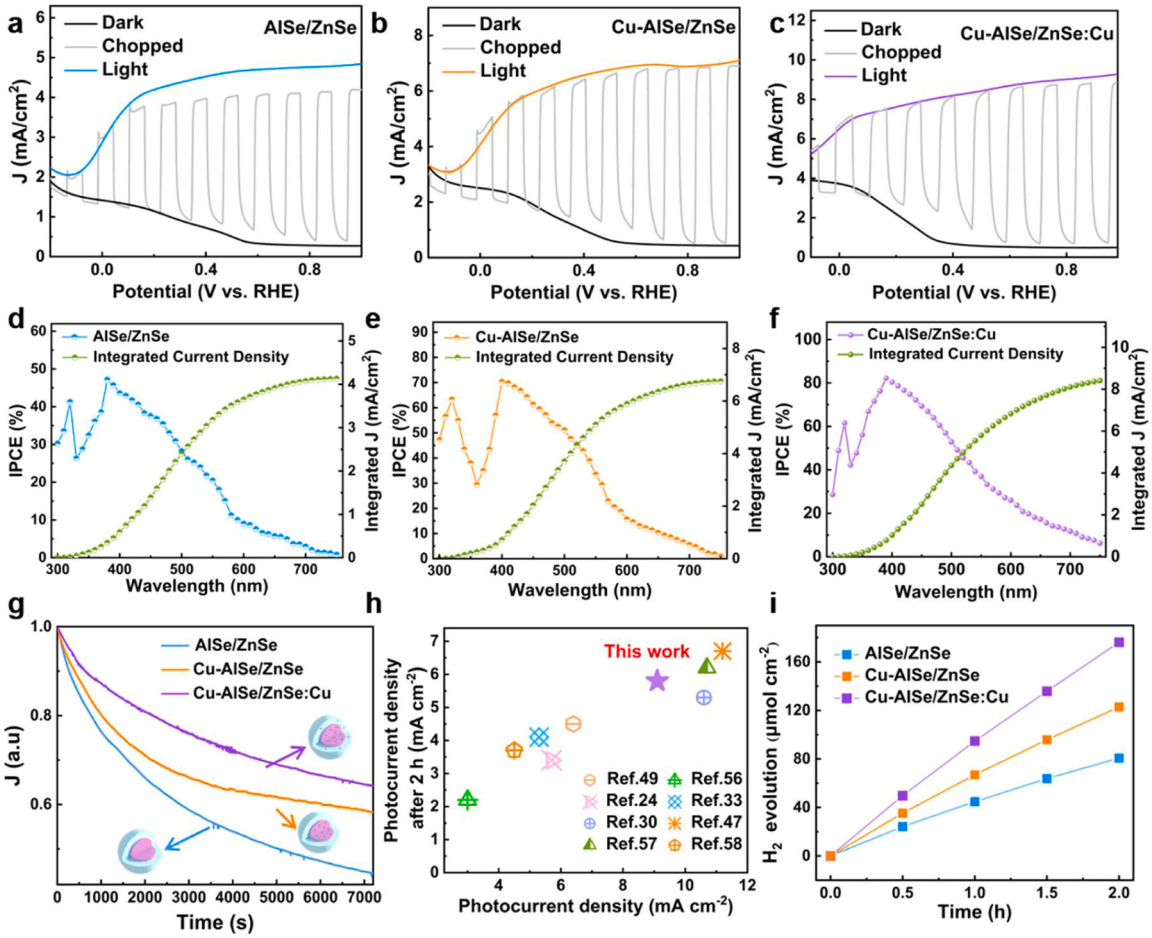

Fig. 5. (a) *J–V* curves for (c) AISe/ZnSe, (b) Cu-AISe/ZnSe and (c) Cu-AISe/ZnSe:Cu QDs-based photoanodes in the dark, under light and chopped illumination (AM 1.5 G, 100 mW cm^{-2}). IPCE spectra for (d) AISe/ZnSe, (e) Cu-AISe/ZnSe and (f) Cu-AISe/ZnSe:Cu QDs-based photoanodes with corresponding integrated current densities. (g) Normalized photocurrent density versus time for the AISe/ZnSe/TiO_2, Cu-AISe/ZnSe/TiO_2 and Cu-AISe/ZnSe:Cu/TiO_2 photoanodes measured at 0.8 V vs. RHE. (h) Performance comparison of the fabricated Cu-AISe/ZnSe:Cu QDs-based PEC device with state-of-the-art eco-friendly QDs-based PEC systems. (i) H_2 evolution rate of AISe/ZnSe, Cu-AISe/ZnSe and Cu-AISe/ZnSe:Cu QDs-PEC cells.

states in the shell enabled efficient holes capture from core QDs for suppressed charge recombination. However, excessive Cu incorporation into the shell further decreased the PEC performance (Fig. S11) owing to the newly induced non-radiative recombination, which is in accordance with the changing trend of QDs' exciton lifetime in Fig. S5**-c**. Moreover, the PEC performance of our QDs-based photoelectrodes without the use of hole sacrificial agents (under neutral conditions) was measured and shown in Fig. S12, still delivering considerable photocurrent densities of ~2.7, 3.6 and 4.4 mA·cm^{-2} for AISe/ZnSe QDs/TiO_2, Cu-AISe/ZnSe QDs/TiO_2 and Cu-AISe/ZnSe:Cu QDs/TiO_2 photoelectrodes, respectively. To explore the effect of ZnS passivation layer thickness on the optimized Cu-AISe/ZnSe:Cu/TiO_2 photoelectrode, the PEC performance of these QDs-sensitized photoanodes coated with 0 and 4 ZnS passivation layers was further measured and shown in Fig. S13, showing saturated photocurrent densities of ~7.7 and 8.5 mA·cm^{-2}, respectively. The suitable ZnS passivation layer thickness has been demonstrated to effectively optimize the photocorrosion of QDs-based PEC cells by passivating the surface trap states and tailoring the band structure for better PEC performance [24].

Furthermore, the incident photon-to-current efficiency (IPCE) spectra and relevant integrated current density of these QDs-photoelectrodes were displayed in Fig. 5**d-f.** In particular, the Cu-AISe/ZnSe:Cu QDs-PEC device showed overall higher IPCE values (ranging from 300–750 nm) than that of the Cu-AISe/ZnSe and AISe/ZnSe QDs-based devices. The integrated current densities from the IPCE curves for AISe/ZnSe, Cu-AISe/ZnSe, and Cu-AISe/ZnSe:Cu QDs-based were calculated to be 4.1, 6.7, and 8.5 mA cm^{-2}, respectively, which agreed well with the experimentally obtained photocurrent densities (Fig. 5**a-c**). The charge transfer kinetics of QDs/TiO_2 photoelectrodes were further unraveled by using the electrochemical impedance spectroscopy (EIS) as shown in Fig. S14 As compared to the EIS Nyquist plots of AISe/ZnSe and Cu-AISe/ZnSe QDs-based photoelectrodes, the Cu-AISe/ZnSe:Cu QDs-based photoelectrode revealed the smallest diameter of the Nyquist semicircle, thus demonstrating the improved interface charge transfer. To explore the photostability of these QDs-based photoelectrodes, the *J-t* curves of the QDs-PEC devices under 2 h light illumination were further tested and displayed in Fig. 5**g**, in which the photocurrent density was normalized to better compare the decay trend of all QDs-photoelectrodes. In general, the possible decay mechanism of the reduced photostability of QDs-based photoanodes can be summarized as: (i) the UV light from solar spectrum could induced holes in TiO_2 as non-radiative recombination centers for photo-oxidation of the QDs, (ii) the degradation of QDs under long-term light irradiation and (iii) the ruin of QDs in corrosive electrolyte (pH~13).

After continuous light irradiation for 2 h, the photocurrent densities of AISe/ZnSe, Cu-AISe/ZnSe and Cu-AISe/ZnSe:Cu QDs-photoelectrodes retained ~45%, 58%, and 64% of their initial values, respectively. The improved stability can be mainly ascribed to the increased electron transfer and hole extraction in the core/shell QDs by synergistic Cu incorporation, which result in the retarded charge recombination and reduced self-oxidation inside the QDs, thereby improving the stability of corresponding QDs-based PEC devices,[53] which were consistent with the charge dynamics analysis in Fig. 4. The obtained device stability and long-term photocurrent density (2-hour illumination) of eco-friendly Cu-AISe/ZnSe:Cu QDs-PEC cell in this work ranked ahead among most of the best reported environment-friendly QDs-PEC systems, as summarized in Fig. 5**h and** Table S4 [56–58]. Furthermore, the optimized PEC performance of as-fabricated QDs-photoanode is even higher than most of the commonly used semiconductor photoanodes (Table S5), indicating that our Cu-AISe/ZnSe:Cu/TiO_2 photoelectrodes are competitive and promising among various PEC devices.

As depicted in Fig. 5**i**, the actual H_2 yield based on our QDs-PEC cells was also detected and quantified by using a gas chromatography (GC) system, showing H_2 generation rates of ~40.4, 61.4 and 88.1 μmol·cm^{-2}·h^{-1} and calculated Faradaic efficiencies (FEs) of 46.2%, 54.1% and 62.4% for AISe/ZnSe, Cu-AISe/ZnSe and Cu-AISe/ZnSe:Cu QDs-based devices, respectively. The results imply the great potential of as-developed environment-friendly Cu-AISe/ZnSe:Cu QDs for high-efficiency PEC hydrogen evolution.

3. Conclusion and perspectives

In conclusion, a novel kind of environment-friendly AISe/ZnSe core/shell QDs with Cu incorporation both in the core and shell region were prepared and utilized as effective light absorbers to achieve high-efficiency solar-driven PEC H_2 production. Both experimental and theoretical investigations unraveled that the Cu incorporation could simultaneously tailor the band structure and carrier kinetics of AISe/ZnSe core/shell QDs for suppressed charge recombination and enhanced carrier extraction efficiency. On the one hand, the Cu incorporation in AISe core resulted in upward conduction band edge position relative to ZnSe shell, thereby inducing the electron delocalization into the shell region and extending the exciton lifetime. On the other hand, Cu incorporation ZnSe shell enabled the introduction of impurity states to capture photogenerated holes from core QDs for retarded charge recombination. As a result, under one sun illumination (AM 1.5 G, 100 mW cm^{-2}), the fabricated Cu-AISe/ZnSe:Cu QDs-based PEC device delivered a maximum photocurrent density of 9.1 mA cm^{-2}. These results indicate that synchronous elemental incorporation in eco-friendly core/shell QDs is a promising strategy towards cost-effective, environment-benign, and high-performance solar energy conversion devices.

CRediT authorship contribution statement

Tong Xin: Data curation, Investigation, Supervision, Writing – original draft. **Xia Li:** Conceptualization, Data curation, Formal analysis, Writing – original draft. **Vomiero Alberto:** Funding acquisition, Supervision, Writing – review & editing. **Jin Lei:** Data curation, Formal analysis, Investigation, Methodology, Supervision. **Cai Mengke:** Data curation, Formal analysis, Investigation, Writing – original draft. **Wang Zhiming M.:** Conceptualization, Funding acquisition, Supervision, Writing – review & editing. **Long Zhihang:** Data curation, Formal analysis, Investigation, Methodology. **Yao Yisen:** Data curation, Formal analysis, Validation, Visualization.

Declaration of Competing Interest

The authors declare that they have no known competing financial interests or personal relationships that could have appeared to influence the work reported in this paper.

Data Availability

Data will be made available on request.

Acknowledgements

X.T. acknowledges the support from National Natural Science Foundation of China (No. 22105031), National Key Research and Development Program of China (No. 2019YFE0121600), Sichuan Science and Technology Program (No. 2021YFH0054, 2023JDGD0011) and Fundamental Research Funds for the Central Universities (ZYGX2020J028). Z.M.W. is grateful to the National Key Research and Development Program of China (No. 2019YFB2203400) and the "111 Project" (No. B20030). A.V. acknowledges the Kempe Foundation, the Knut & Alice Wallenberg Foundation, STINT (Sweden), the Luleå University of Technology (Labfund program), the H2020 Framework program through PNRR iNEST and NEST projects, and Ca' Foscari University of Venice (SPIN project) for financial support. The authors would like to thank Zhang San from Shiyanjia Lab (www.shiyanjia.com) for the DFT analysis.

Appendix A. Supporting information

Supplementary data associated with this article can be found in the online version at doi:10.1016/j.nanoen.2024.109302.

References

[1] L.J. Cushing, S. Li, B.B. Steiger, J.A. Casey, Nat. Energy 8 (2023) 52–61.
[2] A. Rahman, O. Farrok, M.M. Haque, Renew. Sust. Energ. Rev. 161 (2022) 112279.
[3] P. Zhou, I.A. Navid, Y. Ma, Y. Xiao, P. Wang, Z. Ye, B. Zhou, K. Sun, Z. Mi, Nature 613 (2023) 66–70.
[4] T.S. Teitsworth, D.J. Hill, S.R. Litvin, E.T. Ritchie, J. Park, J.P. Custer Jr, A. D. Taggart, S.R. Bottum, S.E. Morley, S. Kim, J.R. McBride, J.M. Atkin, J. F., Nat. 614 (2023) 270–274.
[5] C. Liu, N. Zhang, Y. Li, R. Fan, W. Wang, J. Feng, C. Liu, J. Wang, W. Hao, Z. Li, Z. Zou, Nat. Commun. 14 (2023) 4266.
[6] A.M.K. Fehr, A. Agrawal, F. Mandani, C.L. Conrad, Q. Jiang, S.Y. Park, O. Alley, B. Li, S. Sidhik, I. Metcalf, C. Botello, J.L. Young, J. Even, J.C. Blancon, T. G. Deutsch, K. Zhu, S. Albrecht, F.M. Toma, M. Wong, A.D. Mohite, Nat. Commun. 14 (2023) 3797.
[7] P. Reiss, M. Protiere, L. Li, Small 5 (2009) 154–168.
[8] Z. Long, X. Tong, C. Liu, A.I. Channa, R. Wang, X. Li, F. Lin, A. Vomiero, Z. M. Wang, Chem. Eng. J. 426 (2021) 131298.
[9] Z. Li, A.I. Channa, Z.M. Wang, X. Tong, Small 19 (2023) 2305146.
[10] Y. Zhou, M. Celikin, A. Camellini, G. Sirigu, X. Tong, L. Jin, K. Basu, X. Tong, D. Barba, D. Ma, S. Sun, F. Vidal, M. Z.-Rossi, Z.M. Wang, H. Zhao, A. Vomiero, F. Rosei, Adv. Energy Mater. 7 (2017) 1602728.
[11] M. Cai, X. Tong, H. Zhao, X. Li, Y. You, R. Wang, L. Xia, N. Zhou, L. Wang, Z. M. Wang, Small 18 (2022) 2204495.
[12] A. Kargar, Y. Jing, S.J. Kim, C.T. Riley, X. Pan, D. Wang, ACS Nano 7 (2013) 11112–11120.
[13] L. Liccardo, E. Lushaj, L. Dal Compare, E. Moretti, A. Vomiero, Small Sci. 2 (2021) 2100104.
[14] R. Mazzaro, S.B. Bibi, M. Natali, G. Bergamini, V. Morandi, P. Ceroni, A. Vomiero, Nano Energy 61 (2019) 36–46.
[15] K. Qi, B. Cheng, J. Yu, W. Ho, Chin. J. Catal. 38 (2017) 1936–1955.
[16] J.-Y. Xu, X. Tong, L.V. Besteiro, X. Li, C. Hu, R. Liu, A.I. Channa, H. Zhao, F. Rosei, A.O. Govorov, Q. Wang, Z.M. Wang, Nanoscale 13 (2021) 15301–15310.
[17] Y. You, X. Tong, A.I. Channa, H. Zhi, M. Cai, H. Zhao, L. Xia, G. Liu, H. Zhao, Z. Wang, Chem. Eng. J. 452 (2023) 139490.
[18] N. Zhou, H. Zhao, X. Li, P. Li, Y. You, M. Cai, L. Xia, H. Zhi, A.I. Channa, Z. M. Wang, X. Tong, ACS Mater. Lett. 5 (2023) 1209–1218.
[19] Y. Yan, R.W. Crisp, J. Gu, B.D. Chernomordik, G.F. Pach, A.R. Marshall, J. A. Turner, M.C. Beard, Nat. Energy 2 (2017) 1–7.
[20] W.-W. Zhao, R. Chen, P.-P. Dai, X.-L. Li, J.-J. Xu, H.-Y. Chen, Anal. Chem. 86 (2014) 11513–11516.
[21] J. Feng, F. Li, X. Li, X. Ren, D. Fan, D. Wu, H. Ma, B. Du, N. Zhang, Q. Wei, J. Mater. Chem. B 7 (2019) 1142–1148.
[22] V. Veeramani, Y.-H. Chen, H.-C. Wang, T.-F. Hung, W.-S. Chang, D.-H. Wei, S.-F. Hu, R.-S. Liu, Chem. Eng. J. 349 (2018) 235–240.
[23] W.-X. Dai, L. Zhang, W.-W. Zhao, X.-D. Yu, J.-J. Xu, H.-Y. Chen, Anal. Chem. 89 (2017) 8070–8078.
[24] X. Tong, A.I. Channa, Y. You, P. Wei, X. Li, F. Lin, J. Wu, A. Vomiero, Z.M. Wang, Nano Energy 76 (2020) 105062.
[25] A.C. Berends, M.J.J. Mangnus, C. Xia, F.T. Rabouw, Cd.M. Donega, J. Phys. Chem. Lett. 10 (2019) 1600–1616.
[26] F. Li, M. Zhang, D. Benetti, L. Shi, L.V. Besteiro, H. Zhang, J. Liu, G.S. Selopal, S. Sun, Z. Wang, Q. Wei, F. Rosei, Appl. Catal. B-Environ. 280 (2021) 119402.
[27] H. Zhao, W. Wang, X. Li, P. Li, M. Cai, Y. You, R. Wang, A.I. Channa, X. Tong, Z. M. Wang, Adv. Energy Sust. Res 4 (2022) 2200142.
[28] L. Wang, W. Gu, P. Sheng, Z. Zhang, B. Zhang, Q. Cai, Sens. Actuat. B-Chem. 281 (2019) 1088–1096.
[29] X. Long, R. Tong, A.I. Wang, X. Channa, Y. Li, L. You, M. Xia, H. Cai, Z.M. Zhao, Wang, ChemSusChem 15 (2022) e202200346.
[30] H. Guo, B. Luo, J. Wang, B. Wang, X. Huang, J. Yang, W. Gong, Y. Zhou, X. Niu, J. Mater. Chem. A 8 (2020) 24655–24663.
[31] H. Song, Y. Lin, Z. Zhang, H. Rao, W. Wang, Y. Fang, Z. Pan, X. Zhong, J. Am. Chem. Soc. 143 (2021) 4790–4800.
[32] H. Song, Y. Lin, M. Zhou, H. Rao, Z. Pan, X. Zhong, Angew. Chem. Int. Ed. 60 (2021) 6137–6144.
[33] X. Tong, X.-T. Kong, Y. Zhou, F. Navarro-Pardo, G.S. Selopal, S. Sun, A.O. Govorov, H. Zhao, Z.M. Wang, F. Rosei, Adv. Energy Mater. 8 (2018) 1701432.
[34] M.-A. Langevin, A.M. Ritcey, C.N. Allen, ACS Nano 8 (2014) 3476–3482.
[35] D. Deng, L. Qua, Y. Gu, J. Mater. Chem. C. 2 (2014) 7077–7085.
[36] X. Kang, Y. Yang, L. Huang, Y. Tao, L. Wang, D. Pan, Green. Chem. 17 (2015) 4482–4488.
[37] J. Tang, K.W. Kemp, S. Hoogland, K.S. Jeong, H. Liu, L. Levina, M. Furukawa, X. Wang, R. Debnath, D. Cha, K.W. Chou, A. Fischer, A. Amassian, J.B. Asbury, E. H. Sargent, Nat. Mater. 10 (2011) 765–771.
[38] D.O. Scanlon, C.W. Dunnill, J. Buckeridge, S.A. Shevlin, A.J. Logsdail, S. M. Woodley, C.R. Catlow, M.J. Powell, R.G. Palgrave, I.P. Parkin, G.W. Watson, T. W. Keal, P. Sherwood, A. Walsh, A.A. Sokol, Nat. Mater. 12 (2013) 798–801.
[39] X. Li, X. Tong, S. Yue, C. Liu, A.I. Channa, Y. You, R. Wang, Z. Long, Z. Zhang, Z. Zhao, X.-F. Liu, Z.M. Wang, Nano Energy 89 (2021) 106392.
[40] M.A. Abate, J.-Y. Chang, Sol. Energy Mater. Sol. Cells 182 (2018) 37–44.
[41] Z.H. Long, X. Tong, R. Wang, A.I. Channa, X. Li, Y.M. You, L. Xia, M.K. Cai, H. Y. Zhao, Z.M. Wang, Chemsuschem 15 (2022) e202200346.
[42] O.S. Oluwafemi, B.M.M. May, S. Parani, N. Tsolekile, Mater. Sci. Eng. C. 106 (2020) 110181.
[43] D.A.P. Velásquez, F.L.N. Sousa, T.A.S. Soares, A.J. Caires, D.V. Freitas, M. Navarro, G. Machado, J. Power Sources 506 (2021) 230165.
[44] R. Wang, X. Tong, Z. Long, A.I. Channa, H. Zhao, X. Li, M. Cai, Y. You, X. Sun, Z. Wang, Nano Res 15 (2022) 7614–7621.
[45] T. Torimoto, T. Adachi, K.-i Okazaki, M. Sakuraoka, T. Shibayama, B. Ohtani, A. Kudoand, S. Kuwabata, J. Am. Chem. Soc. 129 (2007) 12388–12389.
[46] G. Manna, S. Jana, R. Bose, N. Pradhan, J. Phys. Chem. Lett. 3 (2012) 2528–2534.
[47] B. Luo, J. Liu, H. Guo, X. Liu, R. Song, K. Shen, Z.M. Wang, D. Jing, G.S. Selopal, F. Rosei, Nano Energy 88 (2021) 106220.
[48] H. Zhao, X. Li, M. Cai, C. Liu, Y. You, R. Wang, A.I. Channa, F. Lin, D. Huo, G. Xu, X. Tong, Z.M. Wang, Adv. Energy Mater. 11 (2021) 2101230.
[49] L. Xia, X. Tong, X. Li, A.I. Channa, Y. You, Z. Long, A. Vomiero, Z.M. Wang, Chem. Eng. J. 442 (2022) 136214.
[50] M. Lim, W. Lee, G. Bang, W.J. Lee, Y. Park, Y. Kwon, Y. Jung, S. Kim, J. Bang, Nanoscale 11 (2019) 10463–10471.
[51] H. Guo, J. Liu, B. Luo, X. Huang, J. Yang, H. Chen, L. Shi, X. Liu, D. Benetti, Y. Zhou, G.S. Selopal, F. Rosei, Z. Wang, X. Niu, J. Mater. Chem. C. 9 (2021) 9610–9618.
[52] J. Bang, S. Das, E.-J. Yu, K. Kim, H. Lim, S. Kim, J.W. Hong, Nano Lett. 20 (2020) 6263–6271.
[53] J. Chen, H.B. Yang, H.B. Tao, L. Zhang, J. Miao, H.-Y. Wang, J. Chen, H. Zhang, B. Liu, Adv. Funct. Mater. 26 (2016) 456–465.
[54] G.S. Selopal, H. Zhao, X. Tong, D. Benetti, F. Navarro-Pardo, Y. Zhou, D. Barba, F. Vidal, Z.M. Wang, F. Rosei, Adv. Funct. Mater. 27 (2017) 1701468.
[55] A.I. Channa, X. Tong, J.-Y. Xu, Y. Liu, C. Wang, M.N. Sial, P. Yu, H. Ji, X. Niu, Z. M. Wang, J. Mater. Chem. A 7 (2019) 10225–10230.
[56] X. Tong, Y. Zhou, L. Jin, K. Basu, R. Adhikari, G.S. Selopal, X. Tong, H. Zhao, S. Sun, A. Vomiero, Z.M. Wang, F. Rosei, Nano Energy 31 (2017) 441–449.
[57] S. Li, S.M. Jung, W. Chung, J.W. Seo, H. Kim, S.I. Park, H.C. Lee, J.S. Han, S.B. Ha, I.Y. Kim, S. In, J.Y. Kim, J. Yang, Carbon Energy 5 (2023) e384.
[58] F. Li, M. Zhang, D. Benetti, L. Shi, L.V. Besteiro, H. Zhang, J. Liu, G.S. Selopal, S. Sun, Z. Wang, Q. Wei, F. Rosei, Appl. Catal. B 280 (2021) 19402.

Li Xia received her PhD degree from the University of Electronic Science and Technology of China in Materials Science and Engineering. Her current research mainly focuses on the synthesis of semiconductor colloidal quantum dots for photoelectrochemical hydrogen production.

Xin Tong is a professor at University of Electronic Science and Technology of China. He obtained his B.E. degree in Electronic Science and Technology (2014) and Ph.D. degree in Materials Science and Engineering (2018) from University of Electronic Science and Technology of China (China). His research interests focus on the design and synthesis of colloidal quantum dots and their applications in solar technologies and optoelectronics.

Yisen Yao is currently a PhD graduate jointly trained by the University of Electronic Science and Technology of China (UESTC) and the Yangtze Delta Region Institute (Huzhou) (UESTCYDRI). His research interests include calculations based on Density Functional Theory (DFT), semiconductor materials, and analysis of photoelectric properties.

Zhihang Long is an associate researcher at Institute of Optics and Electronics, Chinese Academy of Sciences. He received his M.S. degree in Chemical Engineering and Technology (2018) from Southwest Petroleum University and Ph.D. degree in Materials Science and Engineering (2022) from University of Electronic Science and Technology of China. His research interests involve colloidal quantum dots and relevant photoelectric devices.

Mengke Cai received his PhD degree in optical engineering from the University of Electronic Science and Technology of China. His current research is mainly focused on photocatalysis, electrocatalysis, and photo-electrocatalysis for clean energy technologies and environmental applications.

Lei Jin received her Ph.D. degree from Institut national de la recherche scientifique in 2019. She was a Joint Postdoctoral at University of Electronic Science and Technology of China and McGill University from 2019 to 2023. Now she is a Postdoctoral Fellow at Southern University of Science and Technology. Her research interests include nano optoelectronic devices utilizing nanomaterials including quantum dots, 2D materials and carbon materials.

Alberto Vomiero is a chair professor of Experimental Physics at the Department of Engineering Sciences and Mathematics, Luleå University of Technology, Sweden and a professor in Industrial Engineering at the Department of Molecular Sciences and Nanosystems, Ca' Foscari University of Venice, Italy. He is leading a multidisciplinary group focusing on the development of advanced nanomaterials for energy and environmental applications, including solar cells, water splitting and photocatalysis. He is a former Marie Curie International Outgoing Fellow of the European Commission, Fellow of the Swedish Foundations, of the American Ceramic Society, of the Royal Society of Chemistry, and several other Societies.

Zhiming M. Wang is a Professor of National Distinguished Experts at University of Electronic Science and Technology of China. He received a B.S. in Applied Physics from Qingdao University (1992), an M.S. in Physics from Peking University (1995), and a Ph.D. in Condensed Matter Physics from the Chinese Academy of Sciences (1998). He is a Fellow of the Optical Society of American (OSA), Fellow of the Royal Society of Chemistry (RSC), Fellow of the Institute of Physics (IoP) and Fellow of the Institution of Engineering and Technology (IET). His research interests include the rational design of semiconductor nanomaterials for optoelectronics.